2021 43rd Annual International Conference of the
IEEE Engineering in Medicine & Biology Society (EMBC)
Oct 31 - Nov 4, 2021. Virtual Conference

Brain-Wide Diffuse Optical Tomography Based on Cap-Based, Whole-Head fNIRS Recording *

Ali F. Khan*, *Student Member*, *IEEE*, Fan Zhang, Han Yuan, *Member*, *IEEE*, Lei Ding, *Member*, *IEEE*

***Abstract*— Diffuse optical tomography (DOT), based on functional near-infrared spectroscopy, is a portable, low-cost, noninvasive functional neuroimaging technology for studying the human brain in normal and diseased conditions. The goal of the present study was to evaluate the performance of a cap-based brain-wide DOT (BW-DOT) framework in mapping brain-wide networked activities. We first analyzed point-spread-function (PSF)-based metrics on a realistic head geometry. Our simulation results indicated that these metrics of the optode cap varied across the brain and were of lower quality in brain areas deep or away from the optodes. We further reconstructed brain-wide resting-state networks using experimental data from healthy participants, which resembled the template networks established in the fMRI literature. The preliminary results of the present study highlight the importance of evaluating PSF-based metrics on realistic head geometries for DOT and suggest that BW-DOT technology is a promising functional neuroimaging tool for studying brain-wide neural activities and large-scale neural networks, which was not available by patch-based DOT. A full-scope evaluation and validation in more realistic head models and more participants are needed in the future to establish the findings of the present study further.**

***Clinical relevance*— Via simulations and experimental evaluation, this work establishes a novel framework to image large-scale brain networks, which benefits the patient population, such as bedridden patients, infants, etc., who otherwise cannot undergo conventional brain monitoring modalities like fMRI and PET.**

I. Introduction

Diffuse optical tomography (DOT) has shown promise in studying brain activity both in humans [1, 2] and animals [3, 4]. In contrast to functional magnetic resonance imaging (fMRI), DOT benefits from low-cost, silent, multi-contrast, fast data acquisitions and high accessibility, inherited from functional near-infrared spectroscopy (fNIRS) [2]. However, the field-of-view (FOV) of DOT systems varies. For example, high-density DOT (HD-DOT) systems employing high-density optode patches [2] have reported FOVs covering limited brain areas such as somatomotor and visual cortices [5] to a large portion of the brain [6]. On the other hand, cap-based sparse optode montages have reported whole-head coverages [1, 7, 8].

Whole-head coverage is needed to study brain-wide neural activations and networks between distributed systems, such as resting-state networks (RSNs) in humans under resting conditions [1, 6, 9, 10]. RSNs are characterized by spontaneous low-frequency oscillations that exhibit temporally-correlated activity among distributed distinct brain regions [11, 12], which provides valuable information about the intrinsic functional organization of the human brain [13]. More importantly, alterations in brain-wide neural activations and networks, e.g., RSNs, have been reported in almost all major neurological and psychiatric disorders [14], suggesting significant clinical values [15]. Therefore, a DOT system with whole-head FOVs should be employed to map brain-wide hemodynamic responses mediated by brain-wide neural activations, with the goal of being able to study inter-regional functional connectivity, similar to fMRI.

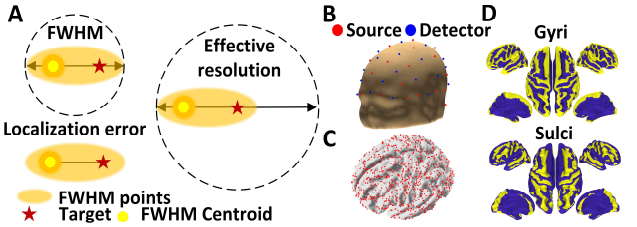

Figure 1. PSF-based metrics defined on a realistic head geometry. (a) PSF-based metric definitions (b) cap-based optode montage (c) points (in red) chosen for the calculation of metrics (d) definitions of shallow (gyri) and deep (sulci) cortical areas in yellow color.

Cap-based DOT systems [1, 7] provide whole-head coverage but have lower spatial resolution than the gold standard HD-DOT systems because of the sparsity of optodes in the former [2]. Recently, we have utilized a cap-based sparse montage covering most of the neocortex to study spatiotemporal activations of the human brain under rest [1] and while performing a motor task [8]. Our promising results have indicated the feasibility and usefulness of the brain-wide DOT (BW-DOT) system in studying the human brain. However, a comprehensive investigation of the spatial resolution of cap-based whole-head systems currently lacks, especially in comparison with patch-based regional DOT systems.

In the present study, we evaluated the performance of the BW-DOT system by quantifying a set of the point-spread function (PSF)-based metrics [16]. These metrics were calculated and analyzed at points sampled across the cortex of a realistic head geometry. We then acquired experimental data from healthy participants under rest and demonstrated the reconstructions of brain-wide RSNs both at group and participant levels. For brevity, investigations corresponding

* This work was supported in part by NSF RII Track-2 FEC 1539068.
A. F. Khan and F. Zhang are with the Stephenson School of Biomedical Engineering, University of Oklahoma, Norman, OK 73019 USA. H. Yuan (e-mail:hanyuan@ou.edu) and L. Ding (e-mail:leiding@ou.edu) are with the Stephenson School of Biomedical Engineering, Institute for Biomedical Engineering, Science and Technology, School of Electrical and Computer Engineering, University of Oklahoma, Norman, OK 73019 USA
*corresponding author email: alifahimkhan@ou.edu

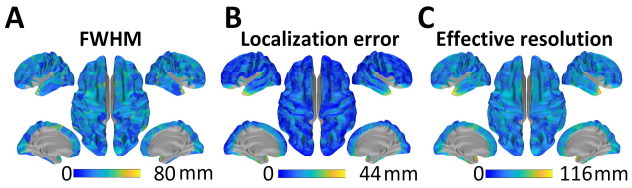

Figure 2. PSF-based metrics projected on cortical surfaces (a) FWHM, (b) localization error and (c) effective resolution. Areas in gray are out of solution source space.

only to deoxygenated hemoglobin (HbR) chromophore changes are reported while oxygenated hemoglobin (HbO) changes were also calculated.

II. Materials and Methods

A. Data Acquisition and Preprocessing

This study was approved by the University of Oklahoma Health Sciences Center Institutional Review Board. Thirteen healthy adult participants (Five females, 31.7 ± 9.3 years) were recruited without any neurological or neuropsychiatric disorders. Two same-day eye-open resting-state data recording sessions, six minutes each, were performed on each individual participant.

Structural head MRIs of participants were acquired using a whole-body 3-Tesla MRI scanner. The fNIRS data were collected by a dual-wavelength ($\lambda 1$ =760 nm, $\lambda 2$ =850 nm) continuous-wave fNIRS system (6.25 Hz, 34 sources, 31 detectors, 109 long channels, eight 8 mm short channels). The optodes were placed on an elastic cap designed with the 10-5 system [17]. The placements of these optodes (Fig. 1b) were designed to be uniformly distributed across the entire scalp to maximize FOV and cover the symmetric brain structures over two hemispheres while maintaining high density (inter-optode distance mean: 3.65 ± 0.44 cm, mode: 2.98 cm, min: 2.98 cm, max: 4.56 cm) (Fig. 1b). The 3D locations of the optode and head landmarks (nasion, left, and right preauricular areas) were recorded using the Polhemus Patriot handheld electromagnetic digitizer (polhemus.com). Data from the peripheral sensors (triaxial accelerometer, pulse oximeter, and breathing belt) were simultaneously recorded at 500Hz. The fNIRS data were pre-processed (bandpass: 0.009 Hz to 0.08 Hz) using an automatic denoising procedure [1, 18, 19].

B. Brain-wide Diffuse Optical Tomography

Participant-specific structural MRI scan data were used to create individual finite element method (FEM) volume meshes [1]. The cortical surface, i.e., the interface of the gray matter and white matter (20,484 nodes), was used for DOT reconstructions, statistical analysis, and visualizations. In simulations, we employed the head MRI from Freesurfer called Bert [20] to create the FEM model using the same procedures as for participants. A spectrally-constrained linear FEM-based forward model linking hemodynamic responses and scalp-based light measurements was used [21] :

$$\vec{y}(t) = A\vec{x}(t) \quad (1)$$

where, the wavelength-dependent observation $\vec{y}(t) = [\Delta\vec{y}_{\lambda 1}(t)\ \Delta\vec{y}_{\lambda 2}(t)]^T$ and the unknown $\vec{x}(t) = \left[\Delta\overrightarrow{HbR}(t)\ \Delta\overrightarrow{HbO}(t)\right]^T$. The vectors $\Delta\overrightarrow{HbR}(t)$ and $\Delta\overrightarrow{HbO}(t)$ are HbR and HbO changes, respectively. The observation

TABLE I PSF-BASED METRICS

	Node Location	**FWHM** (mm)	**Localization error** (mm)	**Effective resolution** (mm)
All nodes	Gyri	(28.1±9.4)	(9.7±6.2)	(41.6±13.8)
	Sulci	(30.2±9.8)	(14.4±6.0)	(48.3±12.5)
	Overall	(29.1±9.7)	(11.9±6.5)	(44.8±13.6)
Within FOV	Gyri	(27.2±8.7)	(5.3±2.9)	(36.0±10.3)
	Sulci	(27.5±9.5)	(5.7±3.4)	(36.8±10.6)
	Overall	(27.3±9.1)	(5.5±3.2)	(36.4±10.5)
Patch-based systems [16]		(21.6±4.6)	(5.3±2.0)	(29.9±5.2)

$\overrightarrow{\Delta y_{\lambda 1}}(t) = -ln\left(\vec{I}_{\lambda 1}(t)/I_{\lambda 1,base}\right)$, where $ln(I(t)/I_{base})$ often called the optical density (OD) is the log-ratio of the measured amplitude of light intensity $I(t)$ on the scalp to the baseline light intensity I_{base}. The forward operator A, a Jacobian was calculated using the NIRFAST software [22]. The OD data (Eq. 1) were subject to the inverse reconstruction using regularized minimum norm estimate[23], yielding the volumetric inverse solution data $\vec{x}(t)$, which were spatially smoothed and projected to the cortical surface to create brain-wide DOT maps.

C. Point-spread function-based metrics in simulations

PSF describes the response of an imaging system to a point input change, i.e., a change of chromophore at a single node of the FEM mesh. We have utilized three PSF-based metrics (Fig. 1a); FWHM, localization error, and effective resolution [16]. Briefly, FWHM describes the maximum Euclidean distance between the nodes with half the amplitude of the maximum-valued node. Localization error represents the mean Euclidean distance between all FWHM points and the simulated node with HbR changes (target node). The effective resolution describes twice the Euclidean distance between the target node and the furthest FWHM node. We simulated a ±10% change in HbR concentration, one by one, at a total of 2879 selected target nodes evenly distributed on the cortical surface (Fig. 1c). The solution space included all FEM nodes less than 45mm from the scalp, excluding non-brain tissues. We first determined the maximum valued node and all the FWHM nodes on each reconstructed BW-DOT map for each simulation. Nodes separated more than 4 mm from each other were considered outliers and were excluded from calculating the metrics. Then all PSF-based metrics were calculated for all simulations.

To investigate the effects of FOV and depth, we reported metric values for nodes according to different criteria separately: nodes within or outside the distance of 25 mm from any optode for FOV and nodes within sulci or gyri (Fig. 1d) [24] for depth].

D. Experimental Data

For experimental data, reconstructed DOT maps were subjected to group-level spatial independent component analysis and statistical correlation tomography [25] to estimate spatial patterns of independent components from inverse tomographic data, each representing an RSN (noted as d-RSNs) [1]. The spatial patterns of these components were matched via visual inspections to a set of previously reported fMRI RSN (noted as f-RSN) templates [26] to perform quantitative evaluations of reconstructed RSNs by BW-DOT. Those components that could not be matched to any f-RSN templates were excluded from further analysis. The matched d-RSNs set included the visual (V), somatomotor (SM), the

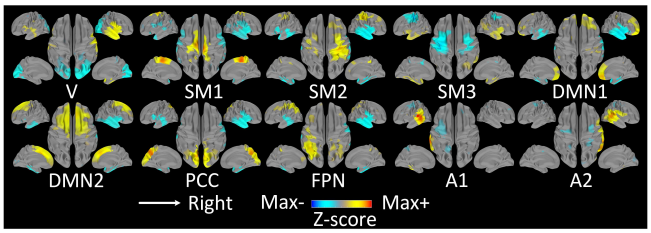

Figure 3. DOT RSNs and their subnetworks from experimental data. All plots are projections on the cortical surface defined as the intersection of the gray and white matter.

default mode network (DMN), frontoparietal network (FPN), auditory (A), and posterior cingulate cortex (PCC) networks. Multiple d-RSNs matched to a single f-RSN template map were defined as subnetworks.

E. Statistical Analysis of DOT RSNs

The spatial pattern similarities between d-RSNs and f-RSN templates were evaluated using the metric of template-matching degree (TD) [27]. The confusion matrices of TD were built at both group and participant levels [1]. The means and standard deviations of TD were calculated from each confusion matrix for three conditions: matched pairs, positive-only unmatched pairs, and unmatched pairs of spatial brain maps. Then the differences between these three conditions were tested for statistical significance using a two-sample t-test (Bonferroni-corrected for multiple comparisons) at the group and participant levels for each RSNs and their subnetworks.

III. Results

A. Simulation Data

The PSF-based metrics were projected and visualized on the cortical surface with interpolation (Fig. 2), yielding a mean of (29.2±9.7) mm, (11.9±6.5) mm, and (44.8±13.6) mm of FWHM, localization error, and effective resolution, respectively (Table 1). Generally, the deeper cortical regions (sulci, Fig. 1d, down) showed higher-valued metrics than shallow cortical regions (gyri, Fig. 1d, up) (Table 1). Some areas with exceptionally high values of metrics included the temporal pole, posterior part of the temporal lobe, ventral parts of the inferior frontal gyrus (IFG), and ventral-medial regions of the superior frontal gyrus (SFG). These parts were mainly outside the cap's FOV. The spatial patterns of all three metrics were bilaterally symmetric with some exceptions, for example, parts of SFG and IFG (Fig. 2a).

All metrics for nodes within the defined FOV were significantly smaller than those away from the optodes. For the nodes within FOV, the differences in the metrics between the sulci and gyri regions were much smaller than those outside FOV (Table 1). For within-FOV nodes, overall, their mean (±std) FWHM, localization error, and effective resolution were 27.3(±9.1) mm, 5.5(±3.2) mm, and 36.4(±10.5) mm, respectively (Table 1). Among these nodes, the gyri nodes (Fig. 1d, up) had the highest quality metrics, i.e., 27.2(±8.7) mm, 5.3(±2.9) mm, and 36.0(±10.3) mm for FWHM, localization error, and, effective resolution respectively, which reach comparable values computed for a patch-based optode system calculated on a simplified geometry, i.e., a regional epicortical surface patch [16].

C. Experimental Data

We reconstructed six group-level brain-wide HbR d-RSNs and their subnetworks (a total of ten spatial maps) from experimental data (Fig. 3). The d-RSNs included one V network, three subnetworks of SM, two subnetworks of DMN, one PCC and FPN network, and two subnetworks of A. Several d-RSNs and their subnetworks showed bilateral spatial symmetry (V, SM1,3, DMN1-2, PCC), while others showed hemispheric dominance (SM2, FPN, A1-2). The d-RSNs spanned regional cortical areas (mainly for basic sensory functions) (V, SM, PCC, A) as well as widely distributed cortical areas (DMN, FPN) (mainly for higher-order functions). The spatial distributions of these RSNs collectively covered brain-wide superficial structures of the cortex and resembled fMRI RSNs (f-RSNs) in literature. The spatial maps of d-RSNs showed a high spatial similarity to f-RSN templates at both the group (Fig. 4a-b) and participant level (Fig. 4c).

IV. Discussion

The purpose of the present study was to evaluate the BW-DOT framework in reconstructing networked brain activations based on near-infrared spectroscopy data designed with a cap-based whole-head optode montage. Our simulation data indicate that the proposed BW-DOT system can map neural activations simultaneously for the entire realistic cortex with its performance, based on PSF-based metrics, similar to a previously reported simplified patch-based regional sparse optodes DOT system [16]. Our work further demonstrated its feasibility and performance using real data to reconstruct networked neural activations in humans under awake resting conditions.

We conducted a study to understand the distribution of PSF-based metric values on a realistic head geometry. We used high-quality surface meshes, resulting in a FEM tetrahedral mesh that retained the complex, convoluted shapes of gyri and sulci. Our localization errors are almost identical to data reported from a patch-based DOT only covering limited cortical regions. Our FWHM and effective resolution data are comparable to data from the patch-based DOT but still relatively inferior because of the brain-wide coverage and the consideration of realistic cortical structures, both of which are not considered in the patch-based DOT. Since we used only one head model, a comprehensive simulation-based assessment based on multiple head models is worth investigating. Moreover, only a subset of points was used for calculating the metrics due to the computational demands. In the future, we expect to include more if not all points in the head model's FEM mesh.

The PSF-based metrics showed a dependence on depth, i.e., the metrics were lower in quality in deeper cortical regions (i.e., sulci) than the shallow regions (i.e., gyri). This depth effect was more prominent in cortical areas away from the optodes (outside FOV). This effect was expected due to the reduced sensitivity at nodes outside FOV. A possible solution to this problem is to include more optodes in the cap montage. It is noted that while this FOV (within 25mm) includes parts of the cortical sulcus structures but could not reach deep brain areas like the insular cortex and thalamus. The capability of mapping relatively deep structures (i.e., cortical sulci) might be enabled by long-distance emitter-receiver pairs used for

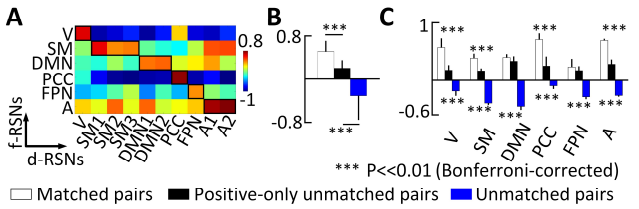

Figure 4. Quantitative evaluation of the spatial patterns of the d-RSNs. (a) Group-level confusion matrices between d-RSNs and f-RSNs template maps for TD spatial matching metric. Matched pairs are enclosed by thick solid lines in diagonals. (b) means and standard deviations of TD (c) Means and standard deviations of TD for individual d-RSNs. All statistical differences were tested using t-test (Bonferroni-corrected).

recordings. However, as PSF-based metrics are sensitive to the factors influencing reconstruction performances, these metrics could be used in a future study to optimize the proposed BW-DOT system. The potential strategies to further improve BW-DOT performance include the use of higher-quality FEM meshes, improved inverse procedures, and optimized optode placement schemes.

Our experimental results demonstrate the reconstructions of multiple brain-wide RSNs simultaneously uncovered from HbR signals. These RSNs collectively covered most of the human neocortex (Fig. 3) and were spatially similar to the RSNs reported in the fMRI literature at both group and participant levels (Fig. 4), thus indicating the potential of the cap-based DOT system in reconstructing brain-wide networked activities. It is important to note that these results are achieved from our current cap-based optode montage covering almost the entire scalp while still providing sufficiently high spatial (73 optodes with an inter-optode distance of 3.65 ± 0.44 cm) and temporal resolutions (6.25 Hz) [8]. Further optimizing the DOT system design using PSF-based metrics discussed above may further improve its performance in mapping brain-wide neural activations and networks.

V. Conclusion

An investigation of PSF-based metrics on realistic head geometries for our proposed cap-based whole-head diffuse optical tomography system suggest comparable performance over sparse optodes patch-based regional systems. These metrics are sensitive to factors that have influences on reconstruction qualities associated with diffuse optical tomography. Furthermore, we demonstrated the simultaneous brain-wide reconstructions of resting-state networks in real data using the proposed BW-DOT resembling fMRI resting-state networks. Therefore, a cap-based whole-head system can be an effective functional neuroimaging tool for monitoring brain-wide neural networks.

References

[1] A. F. Khan, F. Zhang, H. Yuan, and L. Ding, "Brain-wide functional diffuse optical tomography of resting state networks," *Journal of Neural Engineering,* 2021.

[2] M. D. Wheelock, J. P. Culver, and A. T. Eggebrecht, "High-density diffuse optical tomography for imaging human brain function," *Review of Scientific Instruments,* vol. 90, no. 5, p. 051101, 2019, doi: 10.1063/1.5086809.

[3] C. H. Schmitz *et al.*, "Dynamic studies of small animals with a four-color diffuse optical tomography imager," *Review of scientific instruments,* vol. 76, no. 9, p. 094302, 2005.

[4] J. P. Culver, A. M. Siegel, J. J. Stott, and D. A. Boas, "Volumetric diffuse optical tomography of brain activity," *Optics letters,* vol. 28, no. 21, pp. 2061-2063, 2003.

[5] B. R. White *et al.*, "Resting-state functional connectivity in the human brain revealed with diffuse optical tomography," *Neuroimage,* vol. 47, no. 1, pp. 148-156, 2009.

[6] A. T. Eggebrecht *et al.*, "Mapping distributed brain function and networks with diffuse optical tomography," *Nature photonics,* vol. 8, no. 6, pp. 448-454, 2014.

[7] M. A. Franceschini, D. K. Joseph, T. J. Huppert, S. G. Diamond, and D. A. Boas, "Diffuse optical imaging of the whole head," *Journal of biomedical optics,* vol. 11, no. 5, p. 054007, 2006.

[8] A. F. Khan, F. Zhang, H. Yuan, and L. Ding, "Dynamic Activation Patterns of the Motor Brain Revealed by Diffuse Optical Tomography," in *2019 41st Annual International Conference of the IEEE Engineering in Medicine and Biology Society (EMBC)*, 2019: IEEE, pp. 6028-6031.

[9] B. R. White, S. M. Liao, S. L. Ferradal, T. E. Inder, and J. P. Culver, "Bedside optical imaging of occipital resting-state functional connectivity in neonates," *Neuroimage,* vol. 59, no. 3, pp. 2529-2538, 2012.

[10] T. Aihara *et al.*, "Resting-State Functional Connectivity Estimated With Hierarchical Bayesian Diffuse Optical Tomography," *Front Neurosci,* vol. 14, p. 32, 2020, doi: 10.3389/fnins.2020.00032.

[11] B. Biswal, F. Zerrin Yetkin, V. M. Haughton, and J. S. Hyde, "Functional connectivity in the motor cortex of resting human brain using echo-planar MRI," *Magnetic resonance in medicine,* vol. 34, no. 4, pp. 537-541, 1995.

[12] S. L. Bressler and V. Menon, "Large-scale brain networks in cognition: emerging methods and principles," *Trends Cogn Sci,* vol. 14, no. 6, pp. 277-90, Jun 2010, doi: 10.1016/j.tics.2010.04.004.

[13] X. Di, S. Gohel, E. H. Kim, and B. B. Biswal, "Task vs. rest—different network configurations between the coactivation and the resting-state brain networks," *Frontiers in Human Neuroscience,* vol. 7, p. 493, 2013.

[14] R. L. Buckner, J. R. Andrews-Hanna, and D. L. Schacter, "The brain's default network: anatomy, function, and relevance to disease," 2008.

[15] M. D. Fox and M. E. Raichle, "Spontaneous fluctuations in brain activity observed with functional magnetic resonance imaging," *Nat Rev Neurosci,* vol. 8, no. 9, pp. 700-11, Sep 2007, doi: 10.1038/nrn2201.

[16] B. White, "Developing high-density diffuse optical tomography for neuroimaging," 2012.

[17] R. Oostenveld and P. Praamstra, "The five percent electrode system for high-resolution EEG and ERP measurements," *Clin Neurophysiol,* vol. 112, no. 4, pp. 713-9, Apr 2001, doi: 10.1016/s1388-2457(00)00527-7.

[18] F. Zhang, D. Cheong, Y. Chen, A. Khan, L. Ding, and H. Yuan, "Superficial Fluctuations in Functional Near-Infrared Spectroscopy," in *2019 41st Annual International Conference of the IEEE Engineering in Medicine and Biology Society (EMBC)*, 2019: IEEE, pp. 4779-4782.

[19] F. Zhang, D. Cheong, A. F. Khan, Y. Chen, L. Ding, and H. Yuan, "Correcting Physiological Noise in Whole-Head Functional Near-Infrared Spectroscopy," *Journal of Neuroscience Methods,* p. 109262, 2021.

[20] B. Fischl, "FreeSurfer," *Neuroimage,* vol. 62, no. 2, pp. 774-781, 2012.

[21] S. Srinivasan, B. W. Pogue, S. Jiang, H. Dehghani, and K. D. Paulsen, "Spectrally constrained chromophore and scattering near-infrared tomography provides quantitative and robust reconstruction," *Applied optics,* vol. 44, no. 10, pp. 1858-1869, 2005.

[22] H. Dehghani *et al.*, "Near infrared optical tomography using NIRFAST: Algorithm for numerical model and image reconstruction," *Communications in numerical methods in engineering,* vol. 25, no. 6, pp. 711-732, 2009.

[23] M. Bertero, C. De Mol, and E. R. Pike, "Linear inverse problems with discrete data: II. Stability and regularisation," *Inverse problems,* vol. 4, no. 3, p. 573, 1988.

[24] C. Destrieux, B. Fischl, A. Dale, and E. Halgren, "Automatic parcellation of human cortical gyri and sulci using standard anatomical nomenclature," *Neuroimage,* vol. 53, no. 1, pp. 1-15, 2010.

[25] C. Li *et al.*, "Cortical statistical correlation tomography of EEG resting state networks," *Frontiers in neuroscience,* vol. 12, p. 365, 2018.

[26] B. T. Yeo *et al.*, "The organization of the human cerebral cortex estimated by intrinsic functional connectivity," *Journal of neurophysiology,* 2011.

[27] M. D. Greicius *et al.*, "Resting-state functional connectivity in major depression: abnormally increased contributions from subgenual cingulate cortex and thalamus," *Biological psychiatry,* vol. 62, no. 5, pp. 429-437, 2007.